# Constructing Low Dimensional Models of ENSO Part I: The Deterministic Case

Mark S. Roulston [1]
Division of Geological and Planetary Sciences, California Institute of Technology

J. David Neelin
Department of Atmospheric Sciences, University of California, Los Angeles

## Abstract

An intermediate coupled model of the tropical Pacific ocean-atmosphere system was reduced by projecting the nonlinear model onto a truncated basis set of its own empirical orthogonal functions (EOFs). For moderate coupling strengths, the simulated El Niño/Southern Oscillation (ENSO) variability consists of a dominant quasi-quadrennial mode with a period of approximately 4 years and a smaller quasi-biennial mode at a period of approximately 2 years. In the absence of a seasonal cycle, the leading two EOFs capture the dynamics of the leading interannual mode, with a further two EOFs being required to capture the secondary oscillation. The presence of seasonal forcing increases the EOF requirement by two, the leading pair of EOFs being dominated by the annual cycle. Normal mode analysis of the reduced models indicates that the quasi-biennial mode manifests itself, even though it is linearly stable, by nonlinear coupling to the quasi-quadrennial mode. The nonlinearity does not produce the quasi-biennial signal unless the spatial degrees of freedom associated with the linear quasi-biennial mode are present. Other linearly stable modes also couple nonlinearly to the leading interannual mode and to the seasonal cycle, but the quasi-biennial mode is favored over other, less-damped linear modes because of its proximity to a multiple of the quasi-quadrennial frequency.

## Introduction

The use of intermediate coupled models (ICMs) of the tropical Pacific ocean-atmosphere system to study ENSO dynamics is well established [*Zebiak* 1984; *Zebiak and Cane* 1987; *Jin and Neelin* 1993]. Even though such ICMs are less complex than hybrid coupled models and global climate models, they still contain many hundreds of model variables. While these models have relatively high dimensional state spaces, in many parameter regimes they exhibit periodic or quasi-periodic behavior. This suggests that the dynamics actually exist on a low dimensional manifold. Several attempts have been made to construct very low dimensional models of ENSO [*Tziperman et al.* 1994; *Wang and Fang* 1996; *Jin* 1997a; *Jin* 1997b]. These efforts usually begin with an ICM, and then invoke *ad hoc* assumptions to drastically reduce the number of independent model variables. There has also been work with linear reductions of ICMs, especially in the predictability problem [*Blumenthal et al.* 1991; *Xue et al.* 1994]

This paper describes a method for reducing an ICM which is better defined and includes nonlinear interactions. The reduced model is obtained by projecting the ICM onto a truncated set of the model's own empirical orthogonal functions (EOFs). This method has been used in the reduction of atmospheric models [*Rinne and Karhila* 1975; *Selten* 1993; *Selten* 1995; *Selten* 1997a], as well as models of fluid turbulence [*Holmes et al.* 1996].

## ICM Model

### Ocean-Atmosphere Coupling

The ICM used in the study was similar to the model used by *Jin and Neelin* [1993]. The model covers the tropical Pacific. The ocean component is a $1\frac{1}{2}$ layer linearized model on a beta-plane. The atmospheric component is a steady-state, Gill type atmosphere, which also consists of the linearized shallow water equations on a beta-plane [*Gill* 1980]. The details of the model can be found in Appendix A. The atmospheric component of the model is forced by middle tropospheric heating, $Q(x, y)$, which is taken to be a linear function of SST.

$$Q = K_Q T \tag{1}$$

where $K_Q$ has units of $m^2\, s^{-3}\, {}^\circ C^{-1}$.

The windstress, that results from the atmospheric heating, provides the forcing for the ocean, $(\tau_x, \tau_y)$. The dependence of the windstress on the wind velocity was assumed to be linear. The equations are as follows:

$$\tau_x = \rho_a C_D W \mathbf{U} = K_S W \mathbf{U} \tag{2}$$

$$\tau_y = \rho_a C_D W \mathbf{V} = K_S W \mathbf{V} \tag{3}$$

where $\rho_a$ is the atmospheric density, $C_D$ the coefficient of surface drag and $W$ is a characteristic windspeed. The parameters $\rho_a$ and $C_D$ were combined into a single parameter, $K_S$.

The parameter values used are summarized in Table 1.

### Estimating the External Windstress

The windstress can be separated into two components, an *internal* windstress, which is the result of SST forcing within the tropical Pacific, and an *external* windstress which is caused by processes outside the tropical Pacific. The coupled model should be able to generate the internal component but it must be forced with the external windstress. The observed windstress is the sum of the internal and external components. The external

component can be estimated by using the observed SST and the atmospheric model to estimate the internal component, and then subtracting this from the observed windstress. If the observed, external and internal windstresses are represented by $\tau_{obs}$, $\tau_{ext}$ and $\tau_{int}$ respectively, then

$$\tau_{ext} = \tau_{obs} - \tau_{int} \tag{4}$$

If $T_{obs}$ is the observed SST, then $\tau_{int}$ can be estimated using

$$\tau_{int} = K_S W \mathcal{A}(K_Q T_{obs}) \tag{5}$$

where $\mathcal{A}$ is the atmospheric model.

The windstress forcing used was the Florida State University (FSU) pseudo-windstress product covering the period from 1961 to 1991 [*Goldenberg and O'Brien* 1981]. This dataset consists of the pseudo-windstress vectors $(S_x, S_y)$. These are converted into surface windstress using

$$\tau_x = \rho_a C_D S_x \qquad \tau_y = \rho_a C_D S_y \tag{6}$$

The observed SST used was the Reynolds reconstructed SST for the period 1961-1991 [*Smith et al.* 1996]. The SST reconstructions were used, with the atmospheric model described above, to estimate $\tau_{int}$. Since the atmospheric model is linear the product of the two parameters in which there is most uncertainty, $K_Q$ and $W$, can be treated as a single parameter. The value of $K_Q W$ that minimizes the mean square error between the internal zonal windstress anomaly and the observed zonal windstress anomaly was $K_Q = 0.013\, m^3\, s^{-4}\, ^\circ C^{-1}$. With this value, 58% of the observed windstress variance is explained as the internal windstress correlated with tropical Pacific SST. The annual component of the the external windstress was calculated by subtracting the estimated internal windstress from the observed windstress.

## Behavior of the Model

### Nonseasonal Case

The coupled model was forced with a constant windstress, equal to the estimated external windstress for the month of April. April was chosen because the estimated external windstress is most strongly easterly during this month. As the coupling strength, $K_Q$, is increased the model passes through a bifurcation. Below the bifurcation the model does not exhibit self-sustained interannual variability. At a coupling of $K_Q W = 0.0097\, m^3\, s^{-4}\, ^\circ C^{-1}$ the model is just above the bifurcation and exhibits periodic interannual variability. Figure 1 shows a plot of equatorial SST as a function of time. The NINO3 SST oscillates with a period of about 4.5 years and a peak-to-peak amplitude of about 2°C. The longitude-time plot in Fig. 1b shows the spatial pattern of oscillation typical of ENSO, with the SST variance confined to the Eastern Pacific, although the NINO 3 region and the region closest to the eastern boundary are out of phase. This phase difference is not present in observations. The amplitude spectrum of NINO3 SST shows a dominant peak corresponding to a period of about 4.5 years, and a smaller peak corresponding to about 2.1 years. Analysis of observed equatorial Pacific SST has found a quasi-quadrennial (QQ) mode, with a period of 53 months, and a quasi-biennial (QB) mode, with a period of 28 months [*Rasmusson et al.* 1990; *Jiang et al.* 1995; *Aires and Chédin* 2000]. Analysis of the southern oscillation index has also found a low frequency component, with a period of 4-6 years, and a high frequency component with a period of 2-3 years [*Keppenne et al.* 1992]. The similarity of the SST structure of the QB mode with the QQ mode led *Jiang et al.* [1995] to suggest that the QB arises

due to an interaction between the QQ mode and the annual cycle. Since the model used in this study exhibits both a QQ and a QB mode in the absence of seasonal forcing, interactions with the seasonal cycle are clearly not required to explain their existence in this case.

### Seasonal Case

When the model is driven by the seasonally varying external windstress the coupling strength at which the bifurcation occurs increases. Figure 2 shows the behavior of the model with a coupling strength of $K_Q W = 0.0136\, m^3\, s^{-4}\, ^\circ C^{-1}$, which puts it just above the bifurcation. The behavior is more complicated than the case with no seasonal cycle, but there is still a sharp interannual peak. The period of the interannual oscillation is now 5.3 years. The peak-to-peak amplitude of the interannual oscillation is approximately 1°C. Figure 2b shows that the general spatial pattern of ENSO remains although there is more SST variability in the west than in the non-seasonal case. Also visible in the amplitude spectrum, is the annual cycle, as well as several smaller peaks. The seasonal cycle in NINO3 SST in the model has its maximum in January rather than April, as in the observations. In the NINO4 region the annual cycle of SST is 6 months out of phase. This disparity can be explained by recognizing that in the NINO3 region upwelling is important in determining the SST, whereas in NINO4 surface heat flux is more important [*Seager et al.* 1988]. The model includes upwelling and thus does reasonably well in NINO3 but does not include seasonal changes in surface heat flux leading to poor agreement further west. Since the SST variability in the western Pacific is relatively small, failure to reproduce the annual cycle in these regions does not represent a major deficiency in the model. Synchronization with the seasonal cycle is found in observations, with warm events tending to peak between June and November. This does not agree with the observed preference for September to January but the existence of seasonal synchronization demonstrates interaction between the annual cycle and the interannual variability.

## Reduction of the Model

### EOF method

Reducing models by projecting them onto truncated empirical basis sets has been applied to horizontal barotropic models of the atmosphere [*Rinne and Karhila* 1975; *Selten* 1993; *Selten* 1995]. In addition, the method has been used to model convection in the atmospheric boundary layer [*Zhuang* 1996]. More recently, the method has been applied to a horizontal baroclinic model of the atmosphere [*Selten* 1997a]. The approach has also been used to reduce models of turbulence (see *Holmes et al.* [1996]).

There are several variants of the approach. Each constructs the basis sets in a different way. The basis set used here are Empirical Orthogonal Functions (EOFs). The method of EOF analysis was first used in meteorology by Lorenz in 1956 [*Lorenz* 1956]. The method for calculating the EOFs is outlined in Appendix B.

To apply EOF analysis to the output of the coupled model, state vectors must be constructed. The EOF analysis can be applied to each of the fields $u$, $v$, $h$ and $T$ separately but for this work combined state vectors were constructed. To combine the fields into single state vectors, the variables were nondimensionalized. The state vectors used were given

by

$$\mathbf{x} = \left[\frac{\mathbf{u}}{c}, \frac{\mathbf{v}}{c}, \frac{\mathbf{h}}{H}, \frac{\mathbf{T}}{\tilde{T}}\right] \tag{7}$$

where $\mathbf{u}$, $\mathbf{v}$, $\mathbf{H}$, $\mathbf{T}$ are the vectors of coefficients for the fields in the original basis set, $H$ is the mean thermocline depth and $c$ and $\tilde{T}$ are the characteristic scales for speed and SST given by

$$c = \sqrt{g'H} \qquad \tilde{T} = \frac{c\sqrt{\beta c}}{\mu ||\mathcal{A}_x||} \tag{8}$$

where $||\mathcal{A}_x||$ is the norm of the atmospheric model matrix. The windstress forcing was also nondimensionalized using the characteristic windstress given by

$$\tilde{\tau} = \rho H c\sqrt{\beta c} \tag{9}$$

The characteristic scales adopted are not unique but they are found to give satisfactory results.

### Results of the EOF analysis

EOF analysis was performed on the output of the two runs of the coupled model discussed in section 3 above (Figs. 1 and 2). The four leading EOFs are shown in Figs. 3 and 4 for the nonseasonal and seasonally forced cases respectively.

The leading 2 EOFs in Fig. 3 have variability associated with the 4.5 year oscillation. Between them these EOFs contain 95% of the total variance. The h-field components of these EOFs are meridionally symmetric. The T-field components have variability confined largely to the eastern part of the basin, as would be expected for the dominant ENSO mode. The third and fourth EOFs contain a further 4% of the total variance. An inspection of their time series shows that they are dominated by the 2.1 year oscillation, but notice that there is contamination by the 4.5 year mode. This highlights the fact that, because EOFs are constrained to be orthogonal, there is no guarantee that EOF analysis will separate out oscillatory modes of different frequencies, although in this case the QQ and QB modes are quite well separated by projection onto EOFs. The h-field components of EOFs 3 and 4 in Fig. 3 are meridionally asymmetric about the equator, in sharp contrast to the h-field components of EOFs 1 and 2. If broken into symmetric and antisymmetric components, EOFs 3 and 4 have a substantial contribution from each. The distinction between the SST fields of EOFs 1 and 2 and EOFs 3 and 4 is less clear; EOF 3 has a substantial signature in the equatorial cold tongue region. Analysis of observed SST has found that, spatially, the SST variability associated with the QQ mode is similar to that of the QB mode [*Jiang et al.* 1995]. A lack of data precluded a similar analysis of thermocline depth. The results from this model suggest the hypothesis that that QB variability in thermocline depth may be more meridionally asymmetric than that of the QQ mode.

Figure 4 shows the leading EOFs when the model is forced with the seasonally varying external windstress. Now the leading 2 EOFs are dominated by the seasonal cycle, although the time series does show some interannual variability. They account for 91% of the variance (including that of the seasonal cycle). EOFs 3 and 4 contain a further 4% of the variance and are dominated by the interannual variablity, with a period of 5.3 years, although there is contamination by the seasonal cycle. Inspection of the T-field patterns for EOFs 1 and 2 and EOFs 3 and 4 shows that the pattern of SST variability associated with the seasonal cycle is very similar to that associated with the interannual variability. The similar SST patterns found in multiple EOFs

is allowed by the combined field EOF analysis which only dictates that the EOFs of the combined state vectors must be orthogonal. Physically, the similarity of the SST pattern is due to the climatology of upwelling and thermocline depth favoring SST variations in the equatorial cold tongue.

### Projection and Closure

Reduced versions of the full model were constructed by Galerkin projection of the model onto truncated sets of the EOFs, which span a lower dimensional subspace of the statespace of the full model.

Let $\mathbf{P}$ be the matrix of vectors defining the EOFs. That is $[P_{i1}, P_{i2}, ...P_{iN}]$ is the $i$th EOF, where $N$ is the dimension of the model state space. The nondimensionalized model can be written as

$$\frac{d\mathbf{x}}{dt} = \mathbf{M}\mathbf{x} + \mathbf{N}(\mathbf{x}) + \mathbf{F}(t) \qquad (10)$$

where $\mathbf{M}$ represents the linear part of the model, $\mathbf{N}$ represents the nonlinear part and $\mathbf{F}$ is the time dependent forcing. If $\mathbf{y}$ is the reprojected state vector, $\mathbf{y} = \mathbf{P}\mathbf{x}$, then the reprojected model is given by

$$\frac{d\mathbf{y}}{dt} = \mathbf{P}\mathbf{M}\mathbf{P}^T\mathbf{y} + \mathbf{P}\mathbf{N}(\mathbf{P}^T\mathbf{y}) + \mathbf{P}\mathbf{F}(t) \quad (11)$$

The model given by Eq. 11 is exactly equivalent to the model given by Eq. 10 since the basis set has not been truncated. Let the row vectors of $\mathbf{P}$ be ordered in decreasing order of their corresponding eigenvalues. Let $N_r$ be the number of EOFs that are to be retained and let $N_d = N - N_r$ be the number to be discarded. The projection matrix can now be decomposed as follows.

$$\mathbf{P} = \begin{bmatrix} \mathbf{P_r} \\ \mathbf{P_d} \end{bmatrix} \qquad (12)$$

where $\mathbf{P}_r$ is a $N_r \times N$ matrix containing the retained basis vectors and $\mathbf{P}_d$ is a $N_d \times N$ matrix containing the discarded basis vectors. The reprojected state vector, $\mathbf{y}$, can also be decomposed.

$$\mathbf{y} = [\mathbf{y}_r, \mathbf{y}_d] \qquad (13)$$

where $\mathbf{y}_r$ is the vector of the retained components and $\mathbf{y}_d$ is the vector of the discarded components. The truncated, reprojected model is thus given by

$$\frac{d\mathbf{y}_r}{dt} = \mathbf{P}_r\mathbf{M}\mathbf{P}_r^T\mathbf{y}_r + \mathbf{P}_r\mathbf{N}(\mathbf{P}_r^T\mathbf{y}_r) + \mathbf{P}_r\mathbf{F}(t) \qquad (14)$$

The model given by Eq. 14 can be improved by attemping to model the effects of the discarded EOFs on the dynamics of the retained EOFs. The model used is known as the *closure* scheme. Most attempts at constructing closure schemes for truncated models have been statistical-empirical. In most standard atmospheric and oceanic models, the effect of unresolved modes is parameterized by introducing an eddy diffusivity. Essentially the same approach has been used in low order EOF models in which extra linear dissipation is added to prevent model drift [*Selten* 1997a]. The effects of discarded modes isn't always dissipative however. Selten attempted to model the effects of discarded modes by finding linear and quadratic combinations of the retained coefficients that minimized the error in the tendency equations (time derivatives) of the reduced model. This approach was found to improve short range forecasts but led to the model being unstable over longer integration periods [*Selten* 1997b]. Later attempts at this kind of closure attempted to solve the problem of instability by imposing constraints on the closure scheme to bound the total energy of the model [*Achatz and Schmitz* 1997].

In this work a simple closure scheme was adopted. The coefficients of each of the discarded EOFs were specified as constants equal to their mean value in the full model. Let $\bar{\mathbf{y}}_d$ be the vector of the mean coefficients of the discarded EOFs. The projected model thus becomes

$$\frac{d\mathbf{y}_r}{dt} = \mathbf{P}_r\mathbf{M}\mathbf{P}_r^T\mathbf{y}_r + \mathbf{P}_r\mathbf{M}\mathbf{P}_d^T\bar{\mathbf{y}}_d + \mathbf{P}_r\mathbf{N}(\mathbf{P}_r^T\mathbf{y}_r + \mathbf{P}_d^T\bar{\mathbf{y}}_d) + \mathbf{P}_r\mathbf{F}(t) \tag{15}$$

where the terms involving $\bar{\mathbf{y}}_d$ are the closure terms.

## Behavior of the Reduced Models

### Nonseasonal Case

The coupled nonseasonal model was projected onto its leading EOFs, seen in (Fig. 3). We compare behavior for cases where only the two leading EOFs are retained (Fig. 5), and where the four leading EOFs are retained (Fig. 6). In both cases, the pattern of SST variability of the reduced model is very similar to that in the full model. In the four-EOF case, the reduced model captures the QQ mode and the QB mode, as may be seen from the power spectrum (Fig. 6c). The time series shows the QB mode is locked to the dominant QQ mode (Fig. 6a). In the two-EOF case, only the QQ mode is captured (Fig. 5c). This result is consistent with the time series of the EOF coefficients in Fig. 3 but could not entirely be anticipated in advance—in principle, nonlinearity in the two-EOF case could generate QB variability. Apparently, it is much more difficult to do so without the additional spatial structures. The peaks at frequencies higher than the QB seen in Fig. 1c are not reproduced by the reduced model.

To analyse the reduced model it was linearized about its mean state and its normal modes were calculated. The eigenvalues of the normal modes are plotted on the complex plane in Fig. 7. They were calculated for increasing values of coupling. The smallest symbol size represents the uncoupled model projected onto the EOFs of the coupled model, while the largest symbol size represents the full coupling strength used in the coupled model. From Fig. 7 it can be seen that for the standard coupling strength one pair of eigenvalues obtains positive real parts. The point when this pair crosses the imaginary axis represents the Hopf bifurcation, above which the model exhibits sustained interannual oscillations. Notice that for zero coupling the real part of the eigenvalues is close to the coefficient of Rayleigh friction, $r$. This figure thus shows how coupled processes turn a somewhat obscure ocean mode into an unstable and dominant coupled mode. The oscillation period associated with this pair is about 4.5 years; this is the dominant peak in the spectrum of the model shown in Fig. 6c. Figure 7 also shows a second pair of eigenvalues which, for the standard coupling, correspond to a period of about 2.1 years but which have a negative real part indicating that, in the linearized model, this mode of oscillation will be decaying. Fig. 6c does show a peak at this period which represents a sustained oscillatory component. There must be a transfer of energy from the unstable QQ mode to the stable QB model due to non-normal or nonlinear coupling.

Figure 8 shows a case where eight EOFs have been retained in the model. As in Fig. 7, the model has been linearized and the eigenvalues calculated for increasing values of the coupling parameter, starting from the uncoupled case. The time series and spectra for the nonlinear integration of the 8-EOF model (not shown, see Roulston [2000]) exhibit QQ

and QB oscillations, very much like that of the 4-EOF model in Fig. 6. Two of the eigenmodes of the 8-EOF case (Fig. 8) are very similar to the QQ and QB eigenmodes of the 4-EOF case (Fig. 7), although the QB mode is somewhat more strongly decaying. The interesting point in Fig. 8 is that there are two oscillatory modes that are less strongly decaying than the QB mode. However, neither of these modes shows up in the time series of the nonlinear model. The QB mode, despite being more stable, does manifest itself in the spectrum. This must be due to its proximity to a multiple of the frequency of the QQ mode, so that it couples more effectively to the system's only self-sustaining oscillatory mode.

**Seasonal Case**

A similar analysis was performed on the seasonal model. From Fig. 4 it can be seen that the annual cycle and the interannual oscillation are contained in the leading 4 EOFs of the seasonally forced model. The model was projected onto the leading 4 EOFs and forced with the seasonal cycle. The resulting behavior is shown in Fig. 9. It was found that changing the reduced gravity in the reduced model, from $0.0486\,m\,s^{-2}$ to $0.0600\,m\,s^{-2}$, resulted in the reduced model having an interannual frequency closer to the full model. With the standard value the period of the interannual oscillation was about 6.3 years. Figure 9 should be compared with the corresponding full model run shown in Fig. 2. The dominant interannual oscillation and the seasonal cycle are reproduced, but the other peaks in the spectrum shown in Fig. 2c are not present in Fig. 9. This is not suprising since these other oscillations are contained in the higher EOFs. The effect of increasing the number of EOFs included in the model was investigated. The model was projected onto 16 EOFs. The resulting behavior is shown in Fig. 10. The 16 EOF model shows subsidiary peaks similar to the full model, although their amplitudes are not exactly the same. The dominant interannual oscillation is at the same frequency, but its amplitude is more than twice that of the full model. The QB mode is also present, although its amplitude is also too large. The secondary peaks on either side of the seasonal cycle, corresponding to periods of about 1.2 years and 0.8 years, are reproduced, but there is an extra peak at 1.5 years which has negligible amplitude in the full model. Although the 16 EOF reduced model does not reproduce the behavior of the full model *exactly*, it does capture its general dynamics, including relatively minor spectral peaks.

To understand the changes in the spectra of the seasonal model as the number of retained EOFs increases, the normal modes of the linearized models were calculated. These are shown in Figs. 11 and 12. Notice that in both cases *there is only one unstable mode* and it has a period between 4 and 5 years. In the 4 EOF model the other mode has a period very close to 1 year. This mode is excited by the seasonal forcing. In the 16 EOF model one of the extra modes has a period of about 1.25 years; it is still stable but manifests itself because it couples to another mode. Since this mode does not manifest itself in the nonseasonal model, it probably couples to the seasonally driven, 1 year mode, rather than the interannual QQ mode. There are several modes with periods of more than a year. One can be identified with the QB mode of the nonseasonal model. All the peaks in the spectrum in Fig. 2c can be identified with a normal mode in Fig. 12 but all the normal modes remain stable except for the QQ mode.

## Discussion and Conclusions

It is shown that the annual and periodic interannual variability of the ICM can be reproduced with low dimensional models, constructed using truncated basis sets of the model's EOFs. Analysis of these reduced models indicates that the interannual modes of oscillation are modified oscillatory modes of the ocean, which are destabilized by the positive feedbacks associated with ocean-atmosphere coupling. This picture is consistent with previous results [*Neelin and Jin* 1993; *Jin et al.* 1996] which identified the ENSO modes with highly modified ocean scattering modes identified by Moore [*Moore* 1968]. The ocean possesses a spectrum of scattering modes with frequencies in the interannual range. Coupling to the atmosphere modifies these modes, destabilizing some of them. For strong enough coupling a mode becomes unstable and capable of self-sustained oscillations the amplitude of which is bounded by the nonlinearity of the subsurface temperature structure.

The results obtained by normal mode analysis of the reduced models indicates that the QQ mode and the QB mode have their origins in distinct scattering modes of the ocean basin. Furthermore it is not necessarily the case that the QQ and the QB mode are both linearly unstable. For the parameter values used in the model, the first mode to become unstable is the QQ mode, which has a period close to the observed primary ENSO period. A secondary, linearly stable, QB mode is sustained by nonlinear coupling to the primary QQ mode. The QB mode is not the least stable of the linearly stable modes. It manifests itself, while the other modes do not, because the proximity of the QB frequency to the first harmonic of the QQ mode frequency favors the nonlinear coupling. The nonlinearity is not sufficient to create a QB spectral peak if the model is truncated to eliminate the EOFs associated with the QB in the full model. Although, in principle, a nonlinear model with two variables can produce harmonics of a primary oscillation, in this ENSO system the additional spatial degrees of freedom, that permit the existence of a linear QQ mode, are required before the nonlinear coupling can excite this frequency significantly.

The addition of a seasonal cycle enables other linearly stable modes to manifest themselves by coupling to the annual cycle. The low dimensional EOF models are capable of capturing the dynamics of these modes of oscillation. One of the limitations of the EOF models is that they are constructed using the EOFs of the model in a particular point in parameter space. Projecting the ICM onto a particular subset of EOFs is to make an assumption as to what the dominant modes of the model are, an assumption that may not be true for a different set of model parameters.

It has been shown that the modes that manifest themselves in the deterministic case can be reproduced by a relatively small number of EOFs. This supports the use of low-dimensional models for the deterministic case and for the leading ENSO modes, although it suggests that more heuristically derived models such as Jin (1997a) may have trouble in reproducing the nonlinear coupling of the QB mode to the QQ mode. But what of the other interannual modes that are linearly stable and are not sustained by nonlinear coupling to other modes? In a second paper it will be shown that stochastic forcing can excite these stable modes which in turn can couple to the dominant ENSO mode, complicating the study of the impact of stochastic forcing on ENSO.

## Appendix A: The model equations

The model covers the tropical Pacific ocean. The upper layer of the ocean is the mixed layer, of thickness, $H_M$, in which the temperature is constant with depth and is written $T(x,y,t)$. Below the mixed layer is the thermocline layer, with a mean thickness $H_T$. The lower boundary of the thermocline layer is the thermocline with a mean depth $H = H_M + H_T$. The temperature in the thermocline layer is a function of distance from the thermocline interface. Perturbations in the thickness of the thermocline layer will be written as $h(x,y,t)$. The depth averaged zonal and meridional currents in the ocean above the thermocline will be written as $u(x,y,t)$ and $v(x,y,t)$ respectively. The zonal and meridional currents in the mixed layer will be written as $(u_M, v_M)$ and similarly the currents in the thermocline layer will be written as $(u_T, v_T)$. From the above definitions it follows that

$$Hu = H_M u_M + H_T u_T \quad (16)$$

$$Hv = H_M v_M + H_T v_T \quad (17)$$

If the shear velocity is defined as $(u_S, v_S) = (u_M, v_M) - (u_T, v_T)$ then Eqs. 16 and 17 give

$$u_M = u + \frac{H_T}{H} u_S \quad (18)$$

$$v_M = v + \frac{H_T}{H} v_S \quad (19)$$

The dynamical part of the model consists of the linearized shallow-water equations on an equatorial beta-plane.

$$\frac{\partial u}{\partial t} = \beta y v - g' \frac{\partial h}{\partial x} + \frac{\tau_x}{\rho H} - ru \quad (20)$$

$$\frac{\partial v}{\partial t} = -\beta y u - g' \frac{\partial h}{\partial y} + \frac{\tau_y}{\rho H} - rv \quad (21)$$

$$\frac{\partial h}{\partial t} = -H \left( \frac{\partial u}{\partial x} + \frac{\partial v}{\partial y} \right) - rh \quad (22)$$

In Eqs. 20-22 $\beta$ is the gradient of the Coriolis parameter, $g'$ is the reduced gravity, $\rho$ is the mean density of the upper ocean, $r$ is the coefficient of damping by Rayleigh friction and $(\tau_x, \tau_y)$ is the windstress vector at the surface. It is assumed that the shear currents are in equilibrium with the windstress and therefore the following steady state equations for the shear current may be written down

$$qu_S - \beta y v_S = \frac{\tau_x}{\rho H_M} \quad (23)$$

$$qv_S + \beta y u_S = \frac{\tau_y}{\rho H_M} \quad (24)$$

where $q$ is the coefficient of friction between the mixed and thermocline layers. Equations 23 and 24 can be readily solved to give

$$\rho H_M (\beta^2 y^2 + q^2) u_S = q\tau_x + \beta y \tau_y \quad (25)$$

$$\rho H_M (\beta^2 y^2 + q^2) v_S = q\tau_y - \beta y \tau_x \quad (26)$$

The upwelling velocity, $w$, in the mixed layer is given by

$$w = w_T + w_S \quad (27)$$

where $w_T$ and $w_S$ are given by

$$w_T = H_M \left( \frac{\partial u}{\partial x} + \frac{\partial v}{\partial y} \right) \quad (28)$$

$$w_S = H_M \frac{H_T}{H} \left( \frac{\partial u_S}{\partial x} + \frac{\partial v_S}{\partial y} \right) \quad (29)$$

The equation for the mixed layer temperature is

$$\frac{\partial T}{\partial t} = -u_M \frac{\partial T}{\partial x} - v_M \frac{\partial T}{\partial y} + \gamma \mathcal{H}(w) w \frac{(T_B(h) - T)}{H_M} - \alpha T \quad (30)$$

where $\mathcal{H}$ is the heaviside step function, $T_B$ is the temperature at the base of the mixed layer and $\gamma$ is the fraction of upwelling water entrained in the mixed layer. Equation 30 contains all the nonlinear terms of the model, the ocean dynamics are linear.

The temperature at the base of the mixed layer, $T_B$, is parameterized as a function of $h$.

$$T_B = T_0 \tanh\left(\frac{h - h_0}{H^*}\right) - T_0 \qquad (31)$$

Note that for convenience the zero in temperature has been moved. The temperature at the center of the thermocline is about 20°C.

The ocean component is coupled to a steady-state model of the tropical atmosphere [*Gill* 1980; *Gill* 1982] The atmospheric model is linear but it models the response of the tropical atmosphere to SST forcing reasonably well and nonlinear models do not produce substantial improvements [*Allen and Davey* 1993]. The model consists of the linearized shallow-water equations on a beta-plane.

$$-\beta y V + \frac{\partial \phi}{\partial x} + RU = 0 \qquad (32)$$

$$\beta y U + \frac{\partial \phi}{\partial y} + RV = 0 \qquad (33)$$

$$c_a^2\left(\frac{\partial U}{\partial x} + \frac{\partial V}{\partial y}\right) + R\phi = -Q \qquad (34)$$

In Eqs. 32-34 $R$ is the atmospheric damping coefficient, $c_a$ is the atmospheric Kelvin wave speed, $U$ and $V$ are the zonal and meridional components of lower tropospheric wind respectively and $\phi$ is the lower tropospheric geopotential height.

## Appendix B: Calculating EOFs

Let $\mathbf{x}_t = [x_{1t}, x_{2t}, ..., x_{mt}]$ be a state vector with $m$ components which describe the state of the system at a time $t$. Let $\langle \mathbf{x} \rangle$ be the mean state vector and let $\mathbf{x}'_t$ be the deviation of the state vector from the mean at time $t$. The EOF basis is constructed so as to maximize the average projection of the data onto any given number of leading EOF basis vectors under the constraint that the EOF basis vectors be orthonormal. Let $\mathbf{e}_i$ $(i = 1, ..., m)$ be unit vectors defining the new basis. The aim is to maximize $\langle (\mathbf{e}_i^T \mathbf{x}\prime)(\mathbf{e}_i^T \mathbf{x}\prime)^T \rangle$ where $\langle . \rangle$ denotes averaging over the time index. The constraint is that $\mathbf{e}_i^T \mathbf{e}_i = 1$. Thus the function to be maximized is

$$J = \langle (\mathbf{e}_i^T \mathbf{x}\prime)(\mathbf{e}_i^T \mathbf{x}\prime)^T \rangle - \lambda_i(\mathbf{e}_i^T \mathbf{e}_i - 1) \qquad (35)$$

where $\lambda_i$ is the undetermined multiplier. Differentiation of Eq. 35 with respect to $\mathbf{e}_i$ leads to

$$\langle \mathbf{x}\prime \mathbf{x}\prime^T \rangle \mathbf{e}_i = \lambda \mathbf{e}_i \qquad (36)$$

Thus the new basis vectors are the eigenvectors of the matrix $\langle \mathbf{x}\prime \mathbf{x}\prime^T \rangle$. Furthermore,

$$\langle (\mathbf{e}_i^T \mathbf{x}\prime)(\mathbf{e}_i^T \mathbf{x}\prime)^T \rangle = \lambda_i \qquad (37)$$

So the data has the largest average projection onto the eigenvector associated with the largest eigenvalue of $\langle \mathbf{x}\prime \mathbf{x}\prime^T \rangle$. Note that $\langle \mathbf{x}\prime \mathbf{x}\prime^T \rangle$ is a real symmetric matrix and thus it has orthogonal eigenvectors which can be normalized to form a complete orthonormal basis.

Since the mean state vector has been subtracted from the data, $\lambda_i$ is the variance associated with the $i$th basis vector. The essential point about this basis set is that for any value of $D$ more variance is contained in the subspace spanned by the leading $D$ basis vectors than any other $D$-dimensional subspace. These basis vectors are the empirical orthogonal functions of the data set.

**Acknowledgments.** The authors would like to thank Y. Yung for helpful discussions and encouragement. This work was supported by NASA Earth System Science Fellowship NGT5-30068, NSF grant ATM-0082529, and NOAA grant NA86GP0314.

## References


Achatz, U. and Schmitz, G., On the closure problem in the reduction of complex atmospheric models by PIPs and EOFs: A comparison for the case of a two-layer model with zonally symmetric forcing, *J. Atmos. Sci., 54,* 2542-2474, 1997.

Aires, F. and Chédin, A., Independent Component Analysis of multivariate time series: Application to the tropical SST variability, *J. Geophys. Res. (atmos.), 105,* 17437-17455, 2000.

Allen, M.R. and Davey, M.K., Empirical parameterization of tropical ocean-atmosphere coupling: The "inverse Gill problem", *J. Climate, 6,* 509-530, 1993.

Blumenthal, M. B., Predictability of a coupled ocean-atmosphere model. *J. Climate,* **4**, 766–784, 1991.

Gill, A.E., Some simple solutions for heat-induced tropical circulations, *Q.J.R. Met. Soc., 106,* 447-462, 1980.

Gill, A.E., Atmosphere-ocean dynamics, Academic Press, San Diego, 1982.

Goldenberg, S.B. and O'Brien, J.J., Time and space variability of tropical Pacific wind stress, *Mon. Wea. Rev., 109,* 1190-1207, 1981.

Holmes, P., Lumley, J.L. and Berkooz, G., Turbulence, coherent structures, dynamical systems and symmetry, Cambridge Univ. Press, 1996.

Jiang, N., Neelin, J.D. and Ghil, M., Quasi-quadrennial and quasi-biennial variability in the equatorial Pacific, *Clim. Dyn., 12,* 101-112, 1995.

Jin, F.-F. and Neelin, J.D., Modes of interannual tropical ocean-atmosphere interaction - a unified view. Part I: Mumerical results, *J. Atmos. Sci., 50,* 3477-3503, 1993.

Jin, F.-F., Neelin, J.D. and Ghil, M., El Niño/Southern Oscillation and the annual cycle subharmonic frequency-locking and aperiodicity, *Physica D, 98,* 442-465, 1996.

Jin, F.-F., An equatorial recharge paradigm for ENSO I: Conceptual model, *J. Atmos. Sci., 54,* 811-829, 1997.

Jin, F.-F., An equatorial recharge paradigm for ENSO II: a stripped down coupled model, *J. Atmos. Sci., 54,* 830-845, 1997.

Keppenne, C.L., Dettinger, M.D. and Ghil, M., Adaptive filtering and prediction of the southern oscillation index, *J. Geophys. Res., 97,* 20,449-20,454. 1992.

Lorenz, E.N., Empirical orthogonal functions and statistical weather prediction, in *Statistical Forecasting Project*, MIT Press, Cambridge, MA., 1956.

Moore, D.W., Planetary-gravity waves in an equatorial ocean, Ph.D Thesis, Harvard, 1968.

Neelin, J.D. and Jin, F.-F., Modes of interannual tropical ocean-atmosphere interaction - a unified view. Part II: Analytical results in the weak-coupling limit, *J. Atmos. Sci., 50,* 3504-3522, 1993.

Rasmusson, E., Wang, X. and Ropelewski, C., The biennial component of ENSO variability, *J. Mar. Syst., 1,* 71-96, 1990.

Rinne, J. and Karhila, V., A spectral barotropic model in horizontal empirical orthogonal functions, *Q.J.R. Met. Soc., 101,* 365-382, 1975.

Roulston, M.S., Construction of low dimension models of El Niño-Southern Oscillation using empirical orthogonal functions, Ph.D Thesis, California Institute of Technology, 2000.

Seager, R., Zebiak, S.E. and Cane, M.A., A model of the tropical Pacific sea surface temperature climatology, *J. Geophys. Res., 93,* 1265-1280, 1988.

Selten, F.M., Toward an optimal description of atmospheric flow, *J. Atmos. Sci., 50,* 861-877, 1993.

Selten, F.M., An efficient description of the dynamics of barotropic flow, *J. Atmos. Sci., 52,* 915-936, 1995.

Selten, F.M., Baroclinic empirical orthogonal functions as basis functions in an atmospheric model, *J. Atmos. Sci., 54,* 2099-2114, 1997.

Selten, F.M., A statisitcal closure of a low-order barotropic model, *J. Atmos. Sci., 54,* 1085-1093, 1997.

Smith, T.M., Reynolds, R.W., Livezey, R.E. and Stokes, D.C., Reconstruction of historical sea surface temperature using empirical orthogonal functions, *J. Climate, 9,* 1403-1420, 1996.

Tziperman, E., Stone, L., Cane, M.A. and Jarosh, H., El Niño chaos: overlapping resonances between the seasonal cycle and the Pacific Ocean-atmosphere oscillator, *Science, 264,* 72-74, 1994.

Xue, Y., M. A. Cane, S. E. Zebiak and B. Blumenthal, On the prediction of ENSO: A study with a low-order Markov model. *Tellus*, **46**, 512–528, 1994.

Wang, B. and Fang, Z.. Chaotic oscillations of tropical climate: A dynamic system theory for ENSO, *J. Atmos. Sci., 53,* 2786-2802, 1996.

Zebiak, S.E., Tropical atmosphere-ocean interaction and the El Niño/Southern Oscillation phenomenon, Ph.D Thesis, M.I.T., 2000.

Zebiak, S.E. and Cane, M.A., A model of El Niño-Southern oscillation, *Mon. Wea. Rev., 115,* 2262-2278, 1987.

Zhuang, Y., A low-order model of coherent structures in the convective atmospheric surface layer, *Q.J.R. Met. Soc., 122,* 1075-1094, 1996.

M.S. Roulston, Pembroke College, Oxford University,
OX1 1DW, U.K. (e-mail: roulston@maths.ox.ac.uk),
J.D. Neelin, University of California Los Angeles, CA 90095-1565, U.S.A., (e-mail:neelin@atmos.ucla.edu)

[1]Now at Pembroke College, Oxford University, United Kingdom

This preprint was prepared with AGU's LaTeX macros v5.01. File eofensomodel1'v2 formatted October 11, 2001.

**Table 1.** The parameters of the standard model.

| | | |
|---|---|---|
| $\beta$ | planetary vorticity gradient | $2 \times 10^{-11}\, m^{-1} s^{-1}$ |
| $\rho$ | mean density of upper ocean | $1000\, kg\, m^{-3}$ |
| $\rho_a$ | surface density of atmosphere | $1.3\, kg\, m^{-3}$ |
| $L$ | zonal extent of basin | $1.74 \times 10^{7}\, m$ |
| $g'$ | reduced gravity | $0.0486\, m s^{-2}$ |
| $H$ | mean thermocline depth | $150\, m$ |
| $c$ | Kelvin wavespeed $(\sqrt{g'H})$ | $2.7\, m s^{-1}$ |
| $L_0$ | oceanic Rossby radius $(\sqrt{c/\beta})$ | $3.7 \times 10^{5}\, m$ |
| $r$ | upper ocean Rayleigh friction | $(2.5\, years)^{-1}$ |
| $C_D$ | windstress coefficient | $1.5 \times 10^{-3}$ |
| $H_M$ | thickness of mixed layer | $50\, m$ |
| $q$ | mixed layer Rayleigh friction | $(2\, days)^{-1}$ |
| $\alpha$ | oceanic Newtonian cooling coefficient | $(125\, days)^{-1}$ |
| $\gamma$ | entrainment fraction | 0.50 |
| $T_0$ | temperature contrast across thermocline/2 | $10°C$ |
| $h_0$ | temperature structure asymmetry parameter | $40\, m$ |
| $H^*$ | vertical scale of thermocline | $50\, m$ |
| $R$ | atmospheric Rayleigh friction | $(2.3\, days)^{-1}$ |
| $c_a$ | atmospheric Kelvin wavespeed | $60\, m s^{-1}$ |

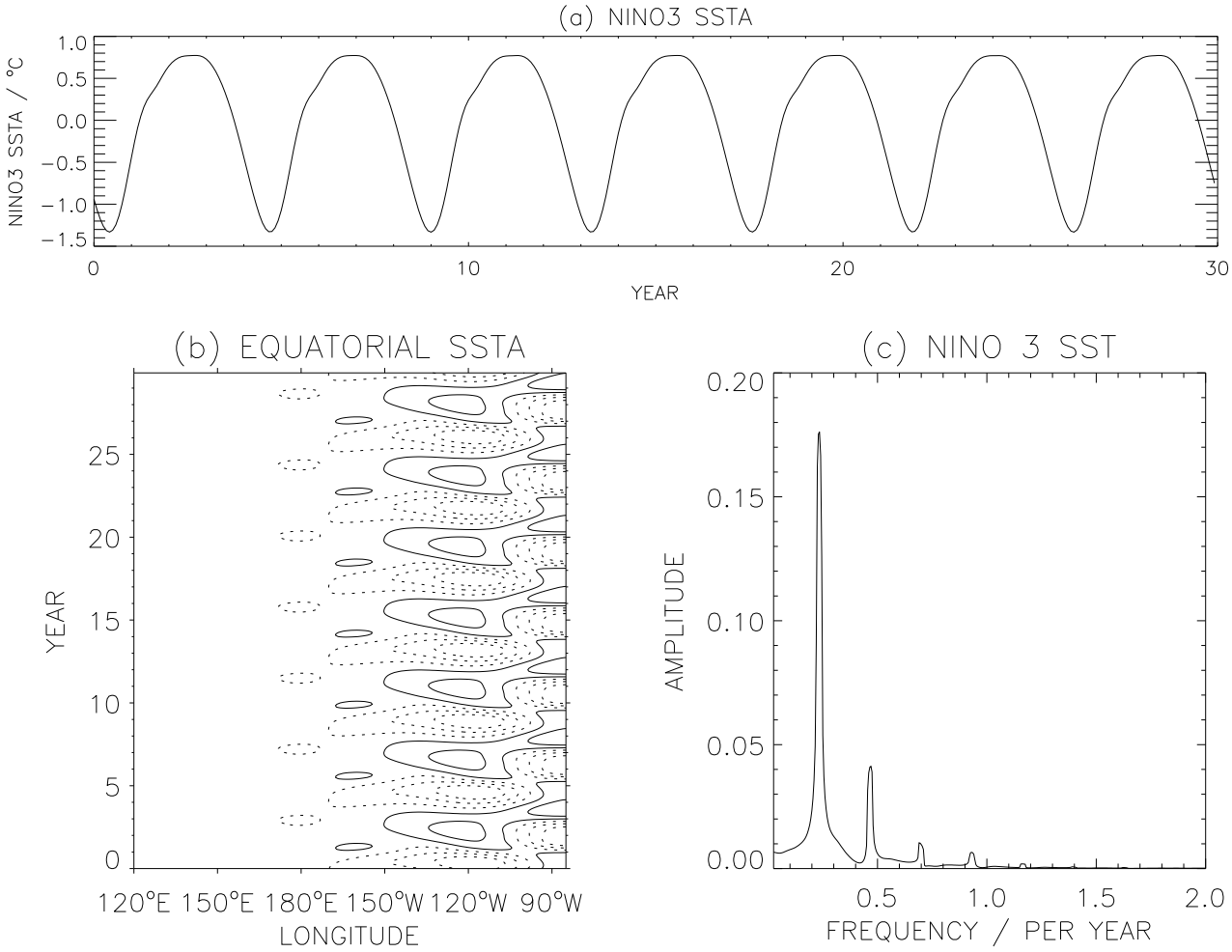


**Figure 1.** The results from the coupled model run forced by the estimated external windstress for April. The coupling was $K_Q W = 0.0097\, m^3\, s^{-4}\, ^\circ C^{-1}$. The spectrum in (c) was calculated from a 200 year run of the model.

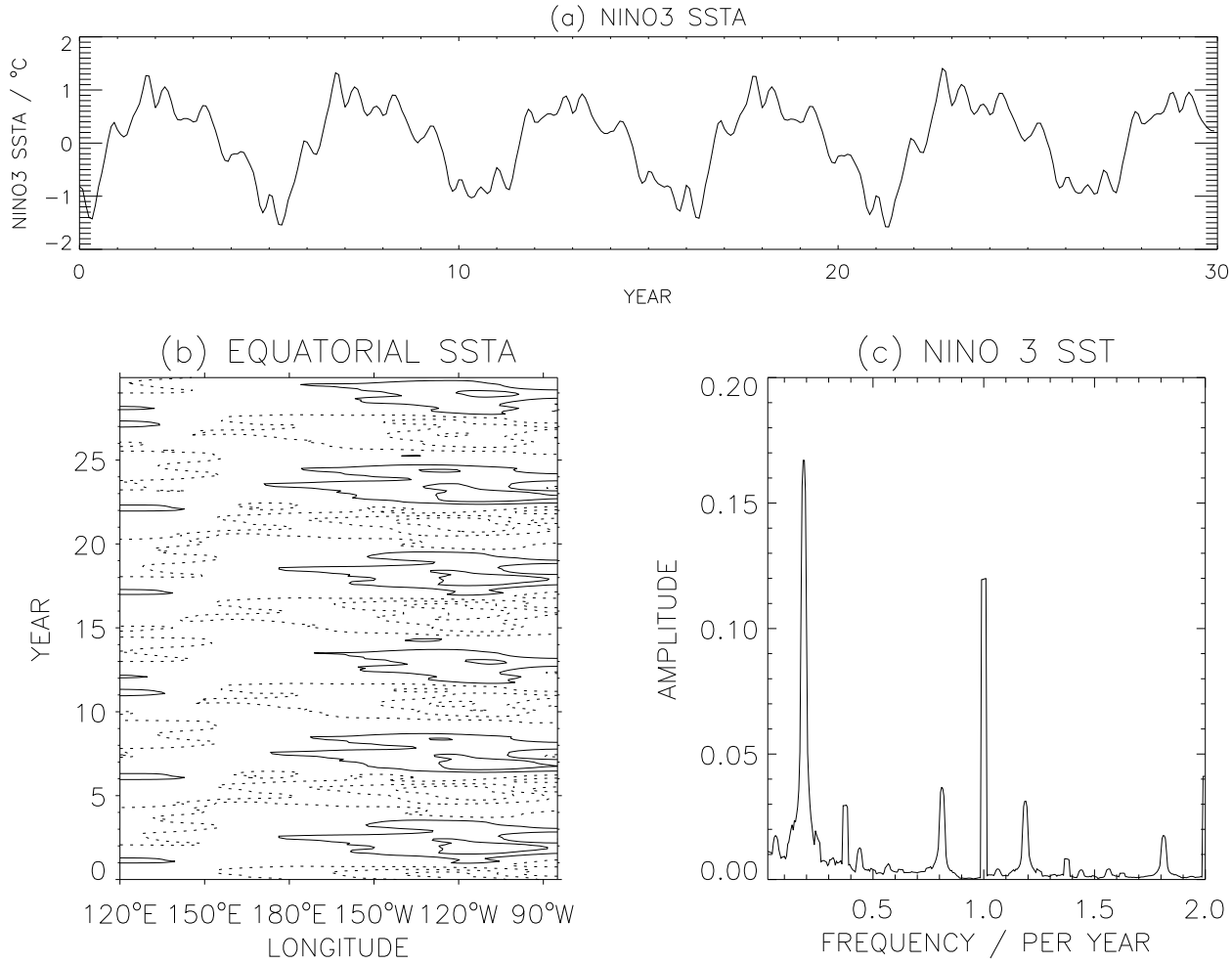


**Figure 2.** The results from a coupled model run forced with the estimated external seasonal windstress. The coupling was $K_Q W = 0.0136\, m^3\, s^{-4}\, ^\circ C^{-1}$. The spectrum in (c) was calculated from a 200 year run of the model.

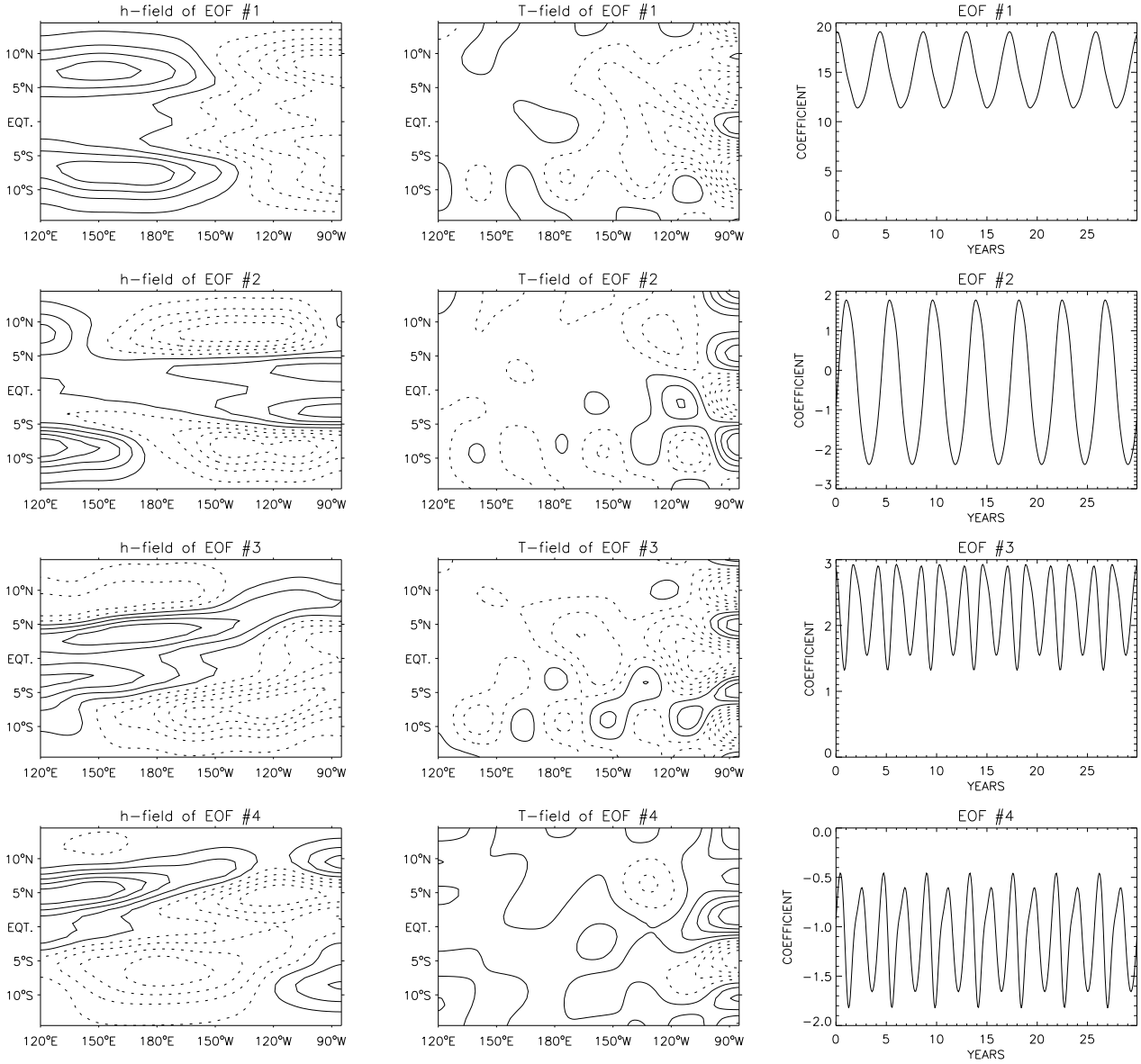


**Figure 3.** The leading EOF patterns associated with the eigenvalues in Fig. 1. The left panels are the h-field components of the leading 4 EOFs, the center panels are the T-field components and the right panels are the time series of the coefficients of the EOF.

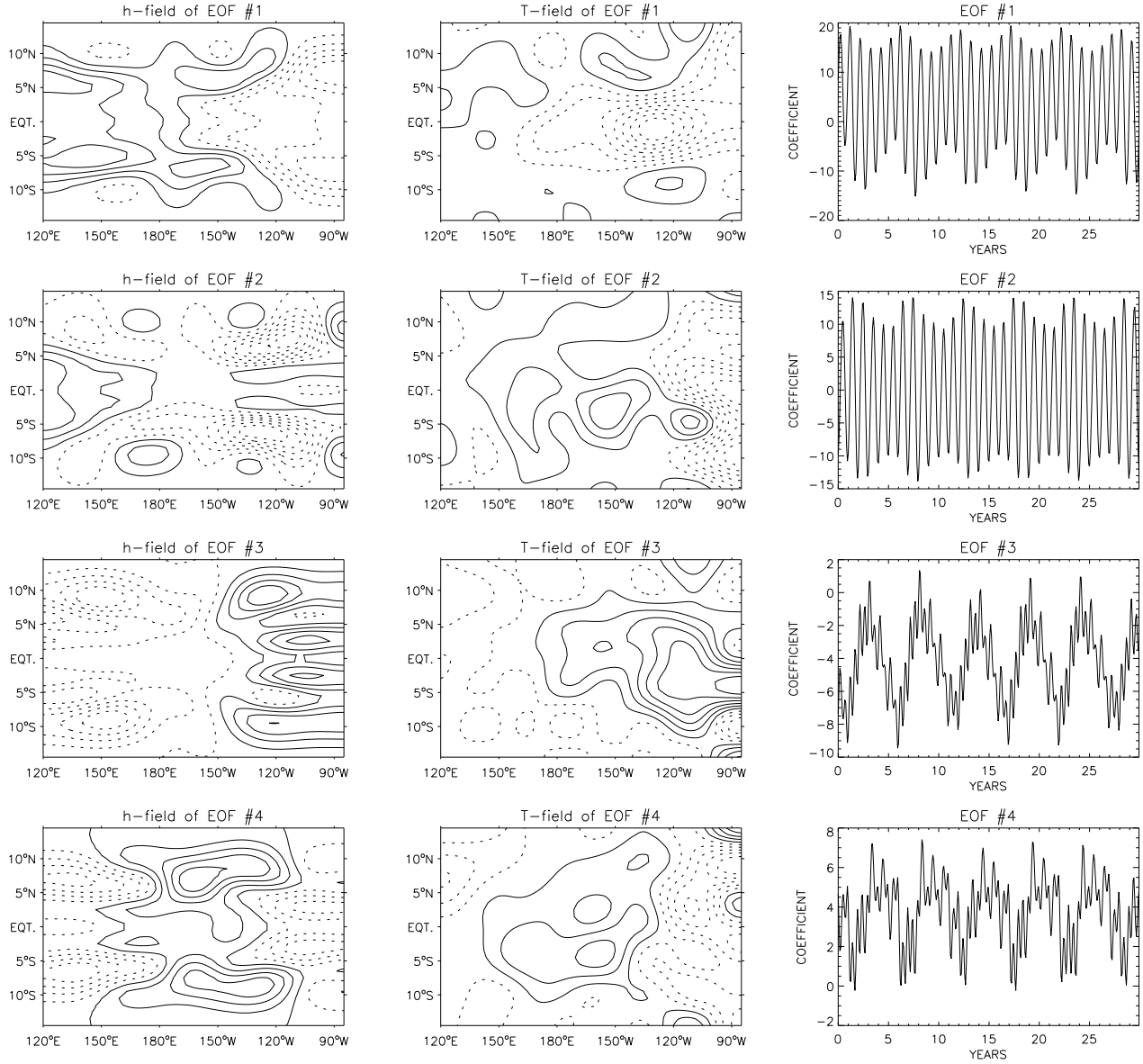


**Figure 4.** As Fig. 3 but for the run shown in Fig. 2.

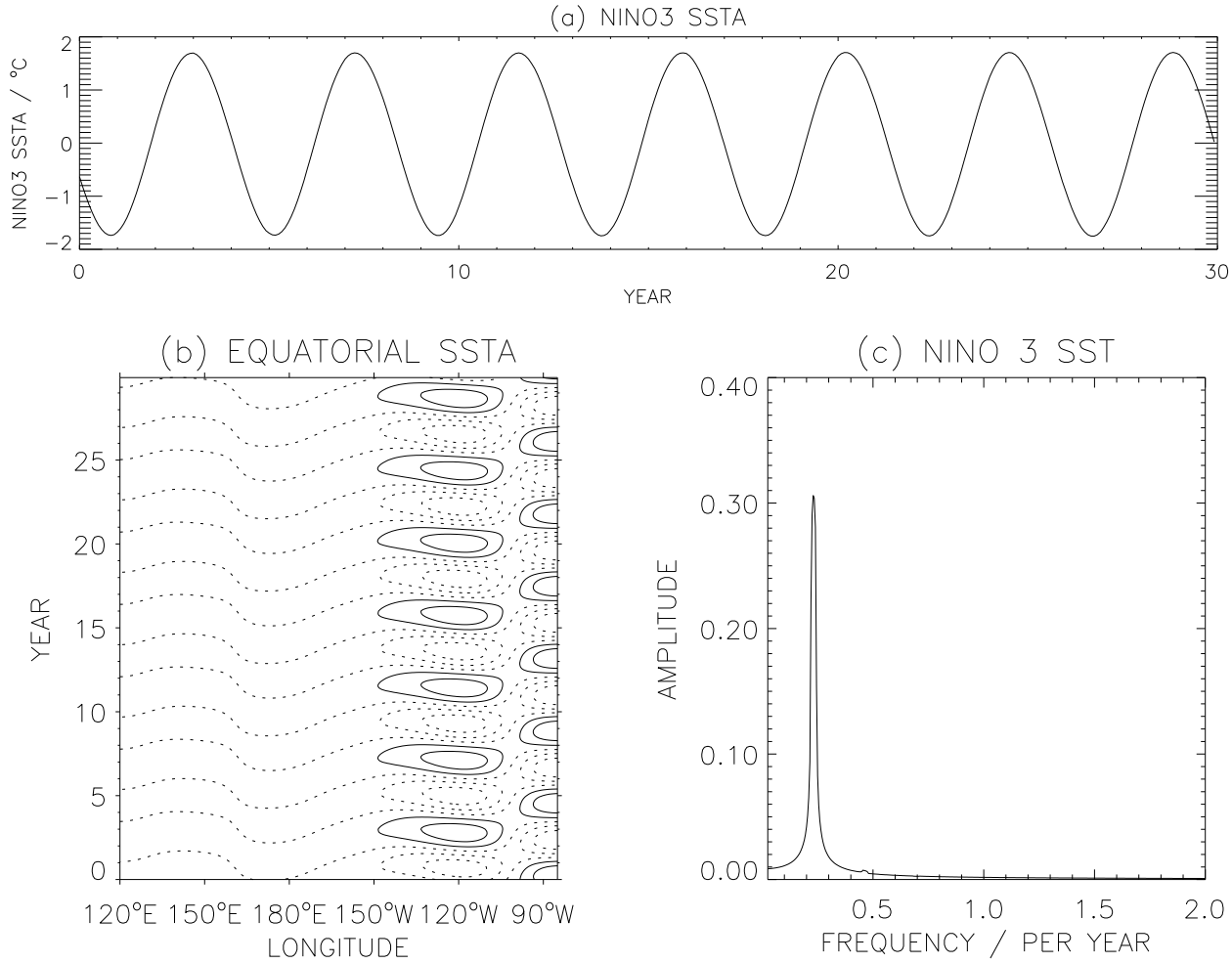


**Figure 5.** The behavior of the 2 EOF model using the leading 2 EOFs in Fig. 3 and a coupling of $K_Q W = 0.0097\, m^3\, s^{-4}\, ^\circ C^{-1}$. The results may be compared to Fig. 1.

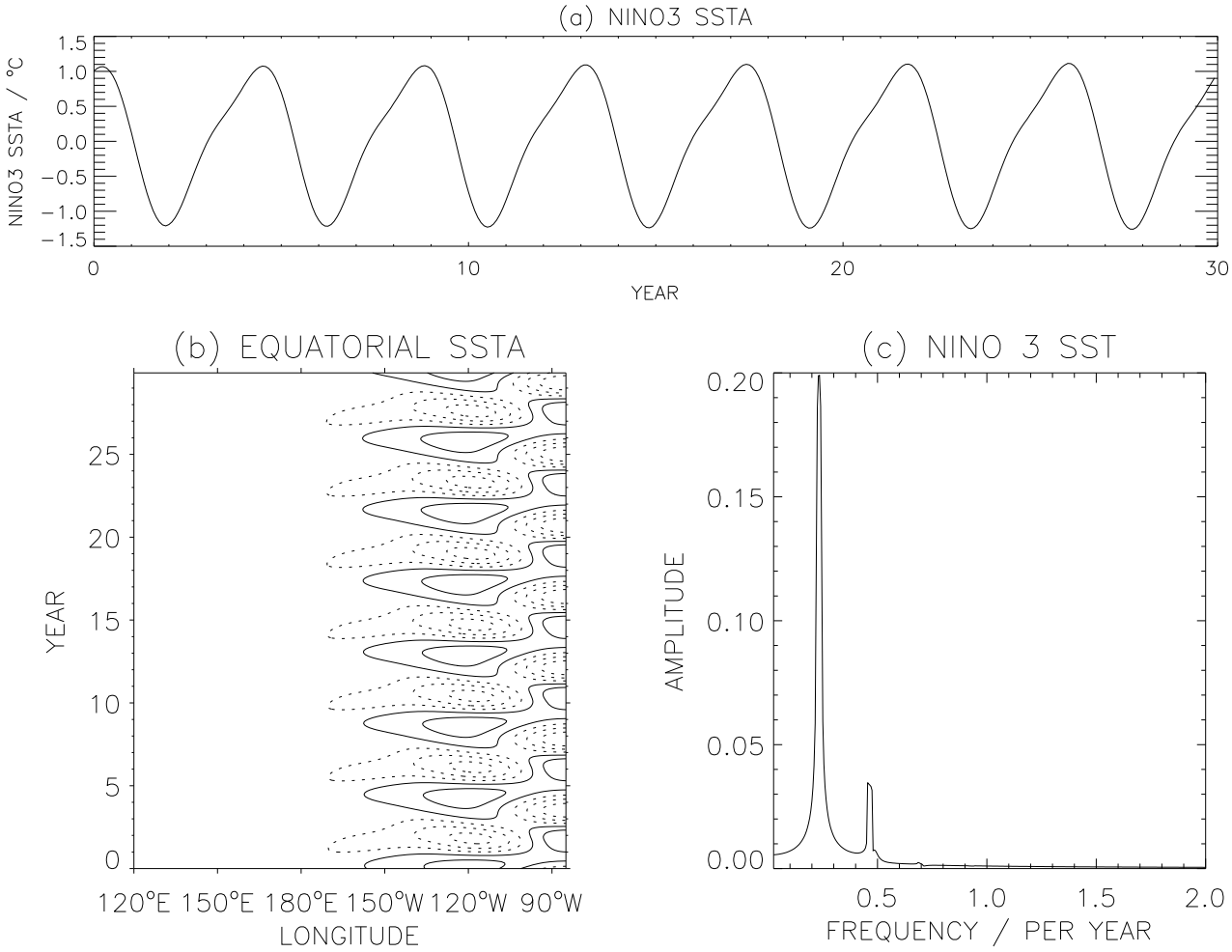


**Figure 6.** The behavior of the 4 EOF model using the leading 4 EOFs in Fig. 3 and a coupling of $K_Q W = 0.0097\, m^3\, s^{-4}\, ^\circ C^{-1}$. The results may be compared to Fig. 1.

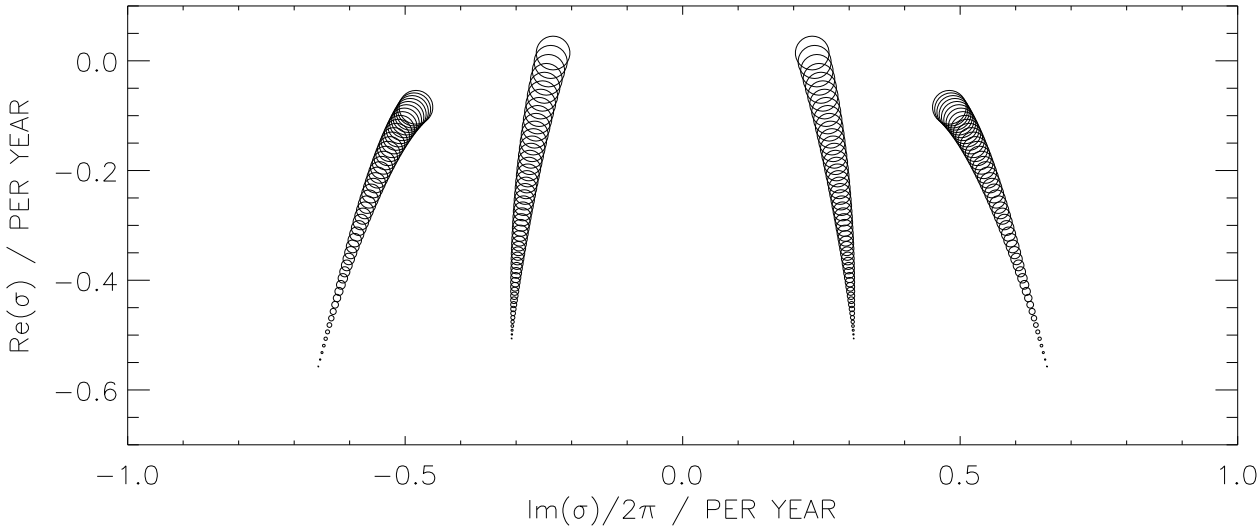


**Figure 7.** The eigenvalues of the normal modes of the 4 EOF reduced model linearized about its mean state. The size of the symbol represents the strength of the coupling ranging from zero to the actual value used in the model.

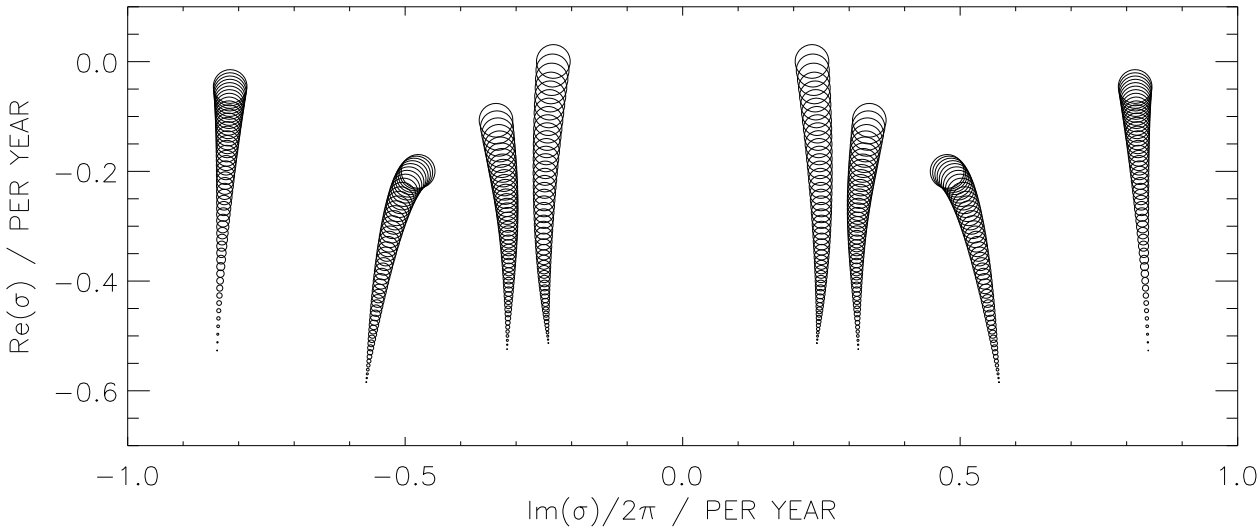


**Figure 8.** As Fig. 7 but for the 8 EOF reduced model.

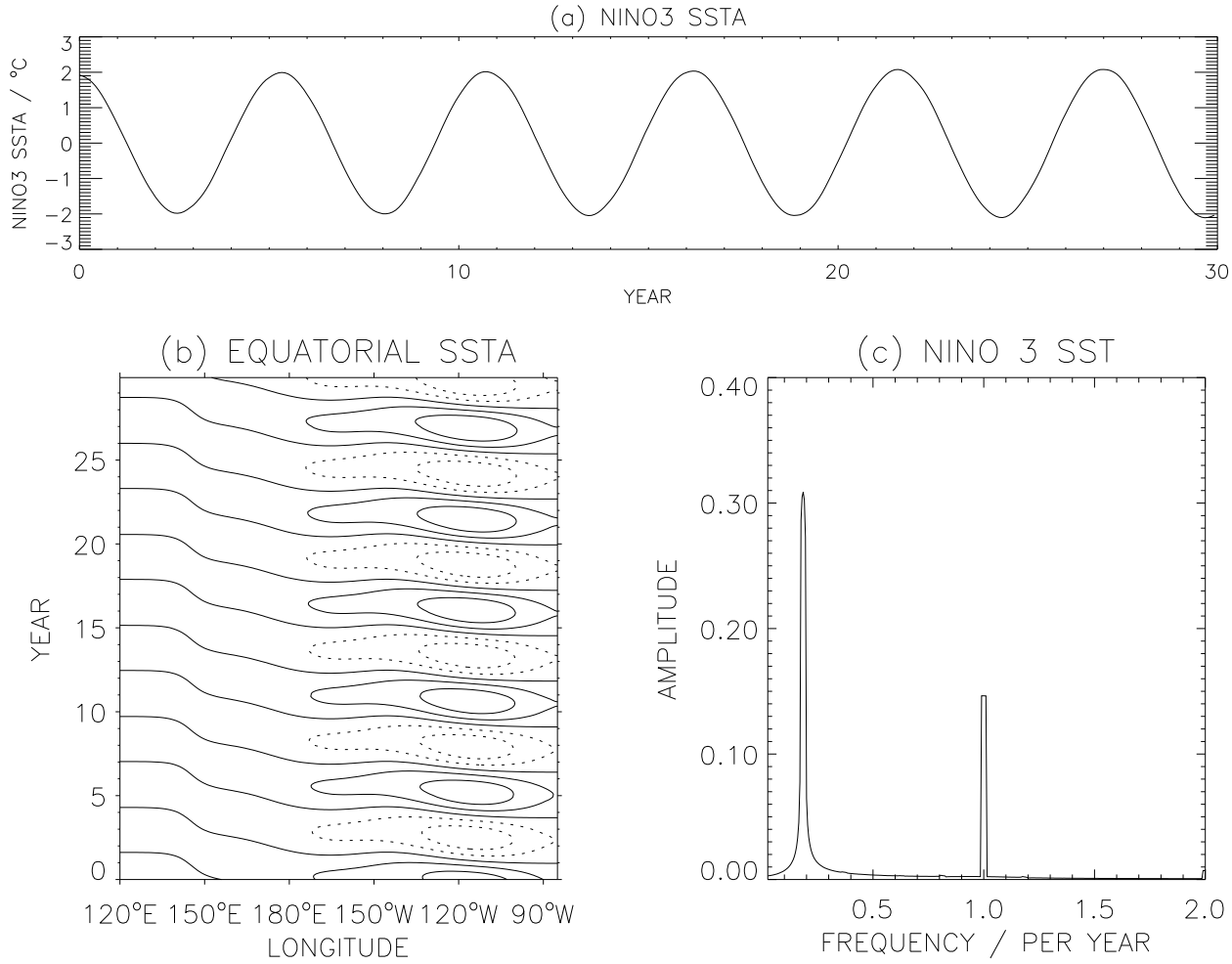


**Figure 9.** The behavior of the 4 EOF model constructed using the leading 4 EOFs in Fig. 4 and a coupling strength of $K_Q W = 0.0136\, m^3\, s^{-4}\, ^\circ C^{-1}$ with seasonal forcing. The results may be compared to Fig. 2.

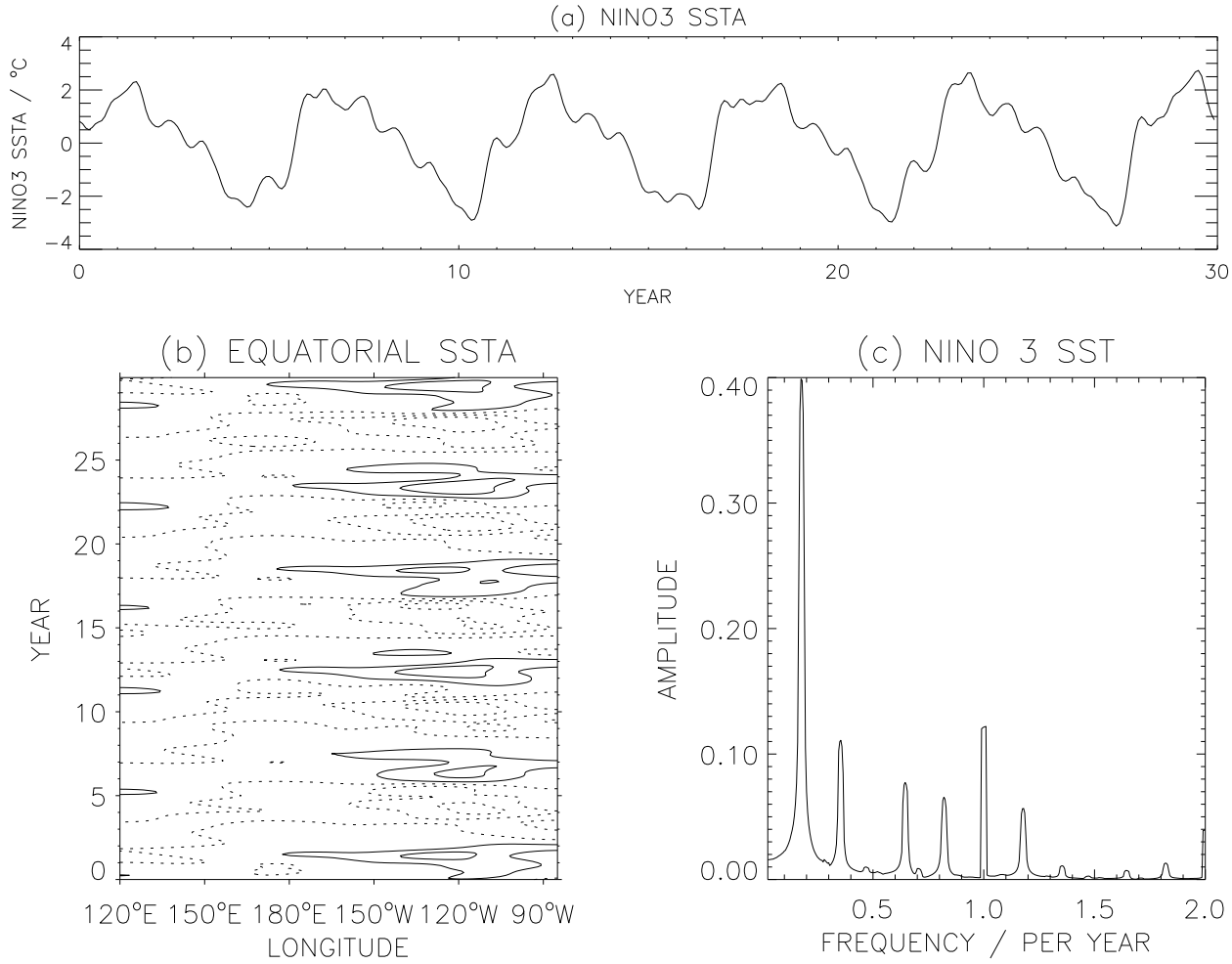


**Figure 10.** As Fig. 9 but with 16 EOFs.

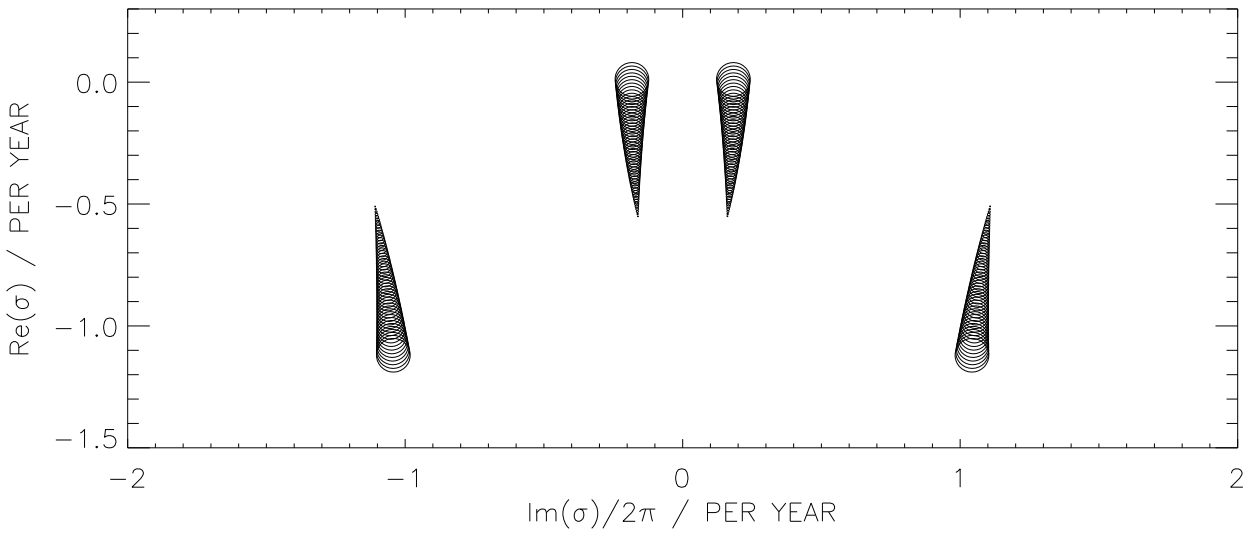


**Figure 11.** The eigenvalues of the normal modes of the 4 EOF reduced seasonally forced model, linearized about its mean state with a coupling strength of $K_Q W = 0.0136\, m^3\, s^{-4}\, ^\circ C^{-1}$. The size of the symbols indicates the strength of the coupling, from zero to the standard value.

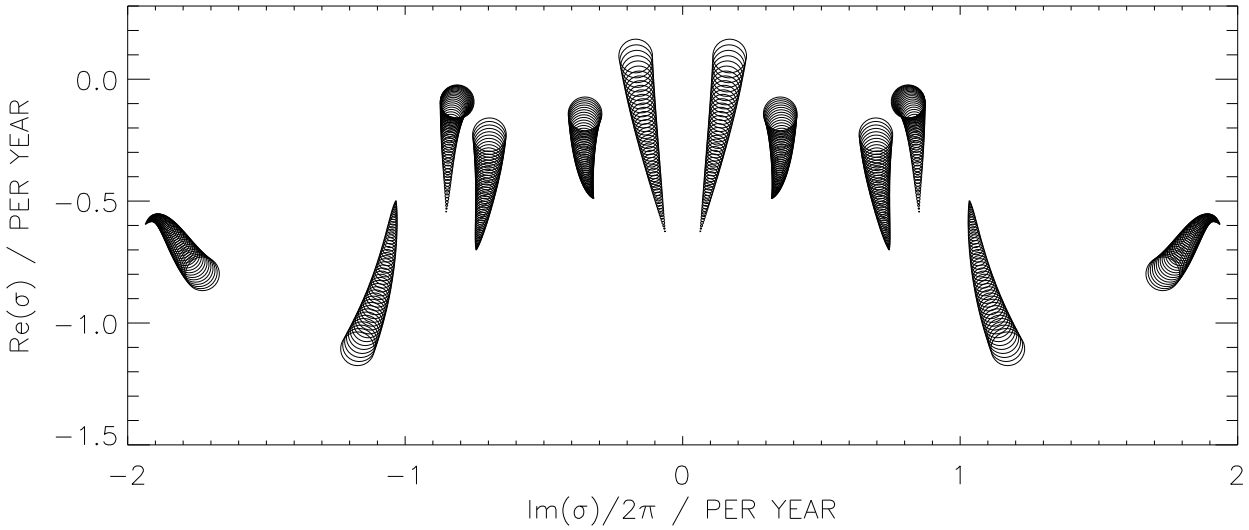


**Figure 12.** As Fig. 11 but for the 16 EOF seasonal model.